Applied Catalysis B: Environmental 147 (2014) 1015–1027

Contents lists available at ScienceDirect

Applied Catalysis B: Environmental

journal homepage: www.elsevier.com/locate/apcatb

Proposed transformation pathway and evolution profile of diclofenac and ibuprofen transformation products during (sono)photocatalysis

I. Michael[a,b], A. Achilleos[a], D. Lambropoulou[c], V. Osorio Torrens[d], S. Pérez[d], M. Petrović[e,f], D. Barceló[e,f], D. Fatta-Kassinos[a,b,*]

[a] Department of Civil and Environmental Engineering, University of Cyprus, PO Box 20537, 1678 Nicosia, Cyprus
[b] Nireas, International Water Research Centre, University of Cyprus, PO Box 20537, 1678 Nicosia, Cyprus
[c] Department of Chemistry, Aristotle University of Thessaloniki, Thessaloniki 54124, Greece
[d] Water and Soil Quality Research Group, Department of Environmental Chemistry, IDAEA-CSIC, Jordi Girona 18-26, 08034 Barcelona, Spain
[e] Catalan Institute for Water Research (ICRA), H2O Building, Scientific and Technological Park of the University of Girona, Emili Grahit 101, 17003 Girona, Spain
[f] Catalan Institution for Research and Advanced Studies (ICREA), PasseigLluisCompanys 23, 08010 Barcelona, Spain

ARTICLE INFO

Article history:
Received 1 August 2013
Received in revised form 14 October 2013
Accepted 15 October 2013
Available online 24 October 2013

Keywords:
Advanced oxidation processes
Diclofenac
Ibuprofen
Transformation products
QToF-MS

ABSTRACT

Liquid chromatography time-of-flight mass spectrometry (UPLC/ESI–QToF–MS) was used for the elucidation of the main transformation products (TPs) resulting from the degradation of diclofenac (DCF) and ibuprofen (IBP) during the application of various advanced oxidation processes in aqueous matrices. The examined processes were TiO_2 photocatalysis driven by UV-A or simulated solar irradiation, sonolysis, and UV-A photocatalysis integrated with ultrasound irradiation (sonophotocatalysis). A comparison between the applied treatment processes was performed with respect to the substrates first-order kinetic rate constant. When compared with sonolysis and UV-A photocatalysis, a higher degradation rate was observed for sonophotocatalysis in the presence of 500 mg L^{-1} TiO_2. Seven TPs of IBP and ten TPs of DCF under UV-A and simulated solar irradiation photocatalysis and sonophotocatalysis, formed by consecutive attack of hydroxyl radicals ($HO^{\bullet}$) in concomitance with the degradation of the primary compounds, were tentatively identified. Overall, no differences were observed in the nature of TPs formed for each substrate among the experiments performed, indicating the involvement of similar reaction mechanisms. The degradation pathway of IBP includes mainly decarboxylation, demethylation and hydroxylation reactions, while the oxidation of DCF, mainly proceeded by oxidation and hydroxylation reactions between chloroaniline and phenylacetic acid. An important observation made during the experiments was that the hydroxylated species (1′-OH-IBP; 2′-OH-IBP; 4′-OH-DCF; 5′-OH-DCF) remained in the solution until 120 min. Finally, the results demonstrated the capacity of the sonophotocatalysis to reduce the initial toxicity of IBP and DCF aqueous solutions against the water flea *Daphnia magna* yielding 20% and 40% immobilization, respectively, at the end of the treatment.

1. Introduction

Concern is growing over the contamination of the aquatic environment with pharmaceutical residues. Research has shown that many pharmaceuticals are not completely removed during conventional wastewater processing techniques, and as a result this has led to their occurrence being reported in wastewater effluents, surface water, and more rarely in groundwater [1,2]. One of the most consumed medications corresponds to the classification of the non-steroidal anti-inflammatory drugs (NSAIDs). NSAIDs have been detected in effluents from hospitals [3] and urban wastewater treatment plants [4–7], in surface water such as rivers and lakes [8,9], as well as in marine waters [10]. Ibuprofen (IBP) and diclofenac (DCF) are often found in the aquatic environment as a result of being one of the most widely used NSAIDs. The domestic route has been identified as the main contamination pathway for IBP and DCF in the aquatic environment [11]. Concentrations of IBP and DCF in surface waters and wastewater effluents have been reported to lie in the ng L^{-1} to μg L^{-1} range [12,13]. As a result, an intensive research has been diverted to the establishment of novel treatment processes particularly for the domestic wastewaters, which are recognized as being the main point discharge source of such substances in the environment [14].

Advanced oxidation processes (AOPs) have received considerable attention during the last several years for their high efficiency to degrade various recalcitrant organic compounds. Among the

* Corresponding author. Tel.: +357 22893515; fax: +357 22895080.
E-mail address: dfatta@ucy.ac.cy (D. Fatta-Kassinos).

0926-3373/$ – see front matter © 2013 Elsevier B.V. All rights reserved.
http://dx.doi.org/10.1016/j.apcatb.2013.10.035

various AOPs, photocatalysis has shown a great potential as a low-cost, environmental friendly and sustainable treatment technology. Heterogeneous photocatalysis based on the interaction of irradiation ($\lambda < 390$ nm) and a semiconductor i.e. titanium dioxide (TiO_2) as a catalyst, is a technology that appears to be a promising tool for water treatment. Another rapidly developing field in AOPs for applications in water remediation is the use of ultrasound irradiation through the generation of cavitation phenomena to destroy or accelerate the destruction of liquid-phase contaminants. Of particular interest is the possibility of coupling ultrasound irradiation with other AOPs like TiO_2 photocatalysis [15].

The degradation of IBP and DCF induced by various AOPs has been widely investigated under different experimental conditions: photocatalysis with TiO_2 [16,17] or Fenton reagent [18], direct photolysis [2,19–21], ozonation [22,23] and sonolysis either alone or combined with UV-A irradiation in the presence of TiO_2 [24,25]. The degradation of the specific substrates was found to depend on several parameters based on the various experimental conditions, which were investigated (e.g. catalyst loading, oxidants addition, ozone dose, ultrasound irradiation, water matrix, etc.).

Several studies have demonstrated the possible negative impact of these compounds in the aquatic environment. IBP has been shown to significantly affect the growth of several bacterial and fungal species [26]. Furthermore, it was found that IBP combined with other environmental pharmaceuticals might impede cell proliferation in human embryonic cells, although IBP cytotoxicity occurred at concentration higher than the values found in the environment [27]. Nonetheless, regarding IBP metabolites, the only information about their potential toxicity is provided by Marco-Urrea et al. [28], who reported 166-fold higher toxicity in water spiked with IBP after being treated with fungi, and where only hydroxylated-IBP metabolites were present.

A characteristic example revealing DCF toxicity, is the global extinction of three species of Gyps vultures (*Gyps bengalensis*, *Gyps indicus* and *Gyps tenuirostris*) in the Indian subcontinent. Use of DCF in animals has been reported to have led to a sharp decline in the vulture population in the Indian subcontinent, a 95% decline in 2003. The mechanism presumably is renal failure, a known side effect of DCF. Vultures eat the carcasses of livestock that have been administered veterinary DCF, and are poisoned by the accumulated chemical, as vultures do not have a particular enzyme to break down DCF [29]. According to Hernando et al. [30], based on the EC_{50} values reported in the literature, DCF may be considered as very toxic to bacteria ($EC_{50} < 1$ mg L^{-1}) and toxic to invertebrates and algae ($EC_{50} = 1–10$ mg L^{-1}). In addition, possible accumulation of DCF in certain organes (muscle, liver, kidneys) was reported [31,32]. DCF is included into the EU priority list of compounds known to pose a significant risk to the aquatic environment [33]. According to the 2012 Commission proposal on priority substances [34], the maximum permitted concentrations of DCF in water set in the environmental quality standards will take effect in 2018, with the aim of achieving good chemical status for this substance by 2027.

Upon partial degradation of pharmaceuticals during wastewater treatment, new chemical entities with different properties, known as transformation products (TPs) may be formed as a consequence of the non-selectivity of $HO^{\bullet}$ that may trigger complex reaction pathways. Understanding the transformation of pharmaceuticals is essential for accurately determining their ultimate environmental fate, conducting accurate risk assessments and improving their removal. The TPs may preserve the same mode of action of the parent compound (i.e. the active moiety remains intact during transformation) and elicit a toxicological effect on non-target organisms in environmental systems either aquatic or terrestrial [35,36]. As the TPs usually occur in a mixture with the parent compound, their contribution to the overall effect cannot be neglected.

The current study investigated the application of liquid chromatography time-of-flight mass spectrometry (UPLC/ESI–QToF–MS) for the elucidation of the main TPs resulting from the TiO_2 photocatalytic degradation of IBP and DCF under either UV-A or simulated solar irradiation and the combined use of UV-A photocatalysis with ultrasound irradiation in aqueous matrices. The main transformation mechanisms have been proposed and a possible degradation pathway for each substrate was developed. A comparison between the applied treatment processes is also provided with respect to the substrates degradation rate constant. The acute toxicity of each substrate and its oxidation products as a whole mixture generated during the treatment process was assessed, and presented herein. According to the authors' knowledge, there is only one study available in the literature revealing data regarding the sonophotocatalytic degradation of IBP [25]. This study focuses on the main operating conditions and the degradation pathway of the compound. The current study focuses on the identification of the main TPs of both IBP and DCF by UPLC/ESI–QToF–MS, along with the proposed transformation pathway of TPs. A further step is the evaluation of the potential toxicity of the parent compounds and their TPs in the different stages of oxidation, something that was not performed so far. It is also noted that a detailed description of the work performed with reference to UV-A and solar-driven TiO_2 photocatalysis for DCF and IBP is provided in Achilleos et al. [37,38].

2. Materials and methods

2.1. Reagents

Analytical grade IBP and DCF (≥99% purity) were purchased from Sigma Aldrich and Dr. Ehrenstorfer GmbH Germany, respectively. LC/MS-grade acetonitrile and methanol (Riedel de Häen, Germany) were used as the organic solvents for the chromatographic analysis, while formic acid and ammonium acetate (ACS grade) were obtained from Merck (Darmstadt, Germany). TiO_2 (Aeroxide® P25), a mixture of 75% anatase and 25% rutile with an average particle size of 21 nm, non-porous with a reactive surface area of 50 m^2 g^{-1} was used for the degradation experiments. For toxicity assays, the treated solutions were neutralized with 2 N NaOH (Merck). Ultrapure water (Millipore, USA) was used throughout the experimental procedures and chromatographic analyses. Solutions containing each compound separately at initial concentration of 10 mg L^{-1} were prepared by dissolving a quantity of the powdered standard in the appropriate volume of the aqueous matrix. This level of concentration, although not environmentally relevant, was used to enable obtaining slower kinetics and to provide favorable conditions for the determination of TPs.

2.2. Experimental setup and procedures

Photocatalytic experiments were performed in an immersion-well, batch-type, laboratory-scale photochemical reactor purchased from ACE Glass Inc. (Vineland, NJ, USA), which is described in detail elsewhere [39]. The reactor was charged with the substrate solution and the catalyst loading ($[TiO_2] = 500$ mg L^{-1}) and the resulting suspension was continuously stirred. The pH of the solution was kept at the inherent pH value. The reactor was connected to a thermostatic bath for maintaining the temperature at the selected value of 25 ± 0.1 °C. Prior to irradiation, the solution was allowed to stay in the dark for 30 min under stirring to reach adsorption equilibrium onto the semiconductor surface. This test was also performed overnight with no further increase in the adsorption. Irradiation was provided using a (i) 9 W UV-A lamp, 3.16 W m^{-2} (Radium Ralutec lamp, 9 W/78, $\lambda = 350–400$ nm,

3.37×10^{-6} einsteins^{-1}), or (ii) laboratory-scale solar simulator (Newport 91193) equipped with 1 kW Xenon lamp and special glass filters restricting the transmission of wavelengths below 290 nm. The irradiation intensity of the simulator was determined using a radiometer Newport type 70260 and it was found 272.3 W m^{-2}.

A digital Sonifier 450 Branson (Emerson Electric Co. US) device equipped with a titanium-made horn tip (diameter = 1.9 cm), operating at 20 kHz was used for the sonochemical experiments (sonolysis). The power intensity emitted in the liquid was in the range of 3.5–8.4 W cm^{-2} as determined calorimetrically [40]. Reactions took place in a cylindrical Pyrex cell under continuous stirring. In those experiments where catalyst was employed (sonocatalytic experiments), the appropriate amount of TiO_2 was added in the solution. Sonophotocatalytic experiments were carried out in a cylindrical Pyrex glass vessel that housed both the ultrasound probe and a UV-A lamp. The digital sonifier described previously was employed for sonication, while the irradiation was provided by a 9 W UV-A lamp. The experimental procedure was similar to that previously described.

During all experiments, samples were periodically withdrawn from the reactor and further analyzed after filtration through a 0.22 μm filter (Millipore, USA). All runs were performed in triplicate and mean values are quoted as results. The relative standard deviation (RSD) of three separate measurements, was never higher than 20%.

The detailed experimental procedures are described in detail elsewhere [37,41].

2.3. Analytical methods

The evaluation of the processes was performed by studying the (%) removal of the examined substrate in solution by UV/Vis spectrophotometry and by monitoring the observed reduction of dissolved organic carbon (DOC) during the processes applied.

UV/Vis spectrophotometry (UV–Vis Jasco V-530) was used to evaluate the conversion of each substrate in the treated samples. The absorbance was measured at the wavelength that corresponds to the maximum of absorbance for each one of the compounds: 220 nm (UV_{220}) for IBP and 276 nm (UV_{276}) for DCF. It is important to note that conversion herein, refers to the degradation of the parent compound (IBP or DCF), but also to that of any oxidation product, that may have similar absorption characteristics. DOC was monitored by direct injection of the filtered samples into a Shimadzu total organic carbon (TOC) analyzer (Shimadzu TOC-$V_{CPH/CPN}$). The calibration was done by injecting standard solutions of potassium hydrogen phthalate.

The treated solutions, withdrawn every 15 min for 2 h, were pre-concentrated by solid phase extraction (SPE) using Oasis® HLB cartridges (6 mL, 200 mg) (Waters Corp., Milford, MA, USA) placed in a filtration equipment (Supelco, Bellefonte, PA). The compounds were eluted by 2×3 mL of pure methanol, and the extracts were concentrated by solvent evaporation with a gentle stream of nitrogen and then reconstituted to a final volume of 1 mL in water/methanol (95:5%, v:v) prior to instrumental analysis. The TPs generated during the treatment processes were monitored by liquid chromatography-time-of-flight mass spectrometry (Micromass QqToF) interfaced with a Waters ACQUITY UPLC system (Micromass, Manchester, UK). Samples from the degradation experiments were separated on a Waters ACQUITY BEH C_{18} column (50×2.1 mm, 1.7 μm particle size) equipped with precolumn (5×2.1 mm) of the same packing material. The mobile phases were: (A) ammonium acetate buffer at pH 6.8 and (B) acetonitrile/methanol (1:1) for IBP, and (A) formic acid 0.05% in water and (B) acetonitrile/methanol (2:1) for DCF. After 1 min of isocratic conditions at 90% A, the portion of A was linearly decreased to 5% within 7 min. These conditions were held for 1 min and then the initial mobile phase composition was restored within 1 min and maintained for column regeneration for another 2 min. The flow rate was 300 μL min^{-1} and the injection volume was 5 μL.

For IBP, the MS analysis was performed with electrospray ionization (ESI) interface in the negative ion mode applying a capillary voltage of −2800 V. The nebulizer gas flow was set to 500 L h^{-1} at a temperature of 300 °C. The drying gas flow was 50 L h^{-1}, and the source temperature was 120 °C. For MS experiments, the instrument operated in the wide pass quadrupole mode with ToF data collected between *m/z* 70 and 400. Tyrosine–valine–tyrosine (Val–Tyr–Val) served as internal lock mass with $[M-H]^- = m/z$ 378.2029.

For DCF, the MS analysis was performed with ESI interface in the positive ion mode applying a capillary voltage of +3500 V. The nebulizer gas flow was set to 50 L h^{-1} and the drying gas flow to 600 L h^{-1} with a temperature of 350 °C. The ToF analyzer was operated at a resolution of 5000 (Full Width at Half Maximum-FWHM) and ESI mass spectra were recorded in 1 s intervals with automatic switching of the dual-sprayer every 10 s for infusion of the internal calibrant for a duration of 1 s. Val–Tyr–Val served as internal lock mass with $[M+H]^+ = m/z$ 380.2185.

All MS data acquisition and processing was done using the software package MassLynx V4.1.

2.4. Ecotoxicity assessment

Toxicity measurements were carried out on samples taken at various time intervals during the treatment processes using the Daphtoxkit F^{TM} magna toxicity test. Toxicity analysis was conducted according to the standard testing protocol using the freshwater species *Daphnia magna* [42] which is described in detail elsewhere [43].

3. Results and discussion

3.1. Degradation kinetics

Besides the examination of photolysis, to allow distinction between degradation and non-destructive disappearance, it was necessary to evaluate also the adsorption of both substrates onto the catalyst surface. Results obtained by the adsorption in the dark and direct photolysis for a time period of 180 min (data not shown) proved that both adsorption (<5%) and photochemical processes (8–10%) were not responsible for the observed fast dissipation when the solutions were irradiated in the presence of TiO_2. Our findings are in accordance with the results of the comprehensive studies of Pérez-Estrada et al. [44] and Méndez-Arriaga et al. [17] showing that no degradation owning to adsorption was observed, while photolytic decomposition of the substrates was neither important. DOC measurements did not show any significant removal (~2%) for the substrates.

The experiments carried out revealed that process efficiency regarding the substrates conversion and DOC removal follows the order: Sonolysis (US) ≈ sonocatalysis < photocatalysis (UV-A and simulated solar irradiation) < sonophotocatalysis. Sonophotocatalysis achieves higher substrates conversion (85% for IBP, 96% for DCF in 2 h) than the individual processes of sonolysis (10% for IBP, 80% for DCF in 2 h) and UV-A photocatalysis (65% for IBP, 21% for DCF in 2 h). It is noted that a detailed description of the work performed with reference to UV-A and solar-driven TiO_2 photocatalysis for DCF and IBP is provided in Achilleos et al. [37,38].

In order to evaluate the kinetics of the substrates degradation under the various experimental conditions, the logarithmic graph $-\ln(C/C_0) = f(t)$ was plotted, the slope of which upon linear

Table 1
Pseudo first-order rate constants that correspond to the photocatalytic (UV-A + TiO_2 or solar + TiO_2), sonolytic (US), sonocatalytic (US + TiO_2) and sonophotocatalytic (UV-A + TiO_2 + US) degradation of 10 mg L^{-1} initial substrate concentration.

Pseudo first-order kinetic constant (k_{app})	Kinetic parameters			
	IBP		DCF	
	($\times 10^{-3}$ min^{-1})	R^2	($\times 10^{-3}$ min^{-1})	R^2
$k_{UVA+TiO_2}$	24.6	0.9910	19.5	0.9943
$k_{solar+TiO_2}$	8.5	0.9956	11.4	0.9945
k_{US}	1.0	0.9898	2.0	0.9913
k_{US+TiO_2}	1.8	0.9977	2.8	0.9897
$k_{UVA+TiO_2+US}$	49	0.9989	40	0.9938

regression yields the apparent rate constant k_{app} (min^{-1}). The experimental data appears to fit well in the linear kinetic equation (data not shown), and consequently IBP and DCF decomposition follows the pseudo first-order kinetic law. The apparent rate constant, k_{app} (min^{-1}), has been chosen as the basic kinetic parameter to compare the different systems, since it is independent of the substrate concentration and therefore, enables to determine the reaction-system activity. Table 1 summarizes the values of k_{app} and the linear regression coefficients (R^2) for all the cases studied herein.

As clearly seen in Table 1, photocatalytic degradation under UV-A or simulated solar irradiation occurs appreciably faster than sonolytic or sonocatalytic degradation. Interestingly, there appears to be a synergistic effect between ultrasound and UV-A irradiation in the presence of TiO_2 since rate constants of the combined process ($k_{UVA+TiO_2+US}$) are greater than the sum of the rate constants of the individual processes ($k_{TiO_2+US} + k_{UVA+TiO_2}$). The synergy can be quantified using the equation adapted from Mrowetz et al. [45], as the normalized difference between the rate constants obtained under sonophotocatalysis and the sum of those obtained under separate UV-A photocatalysis and sonocatalysis. This was found to be 0.46 and 0.44 for IBP and DCF, respectively. The beneficial effect of coupling photocatalysis with sonolysis may be attributed to several reasons i.e. an increased production of $HO^{\bullet}$ in the reaction, enhanced mass transfer of organics between the liquid phase and the catalyst surface, and increased catalytic activity due to ultrasound de-aggregating catalyst particles, thus increasing surface area [25,46]. Noteworthy is that the evaluation of kinetics during the AOPs applied herein, was performed with the aim to be able later on to correlate the intensities of the TPs formed with their potential toxicity. In essence, what can be learnt by the kinetics is how fast the various TPs can be formed, and also at what times of the treatment the potential toxicity related to them can appear.

Photostability of the catalyst is a very important parameter to be assessed since it contributes to the catalyst reuse and therefore to, lowering the operational cost considerably. In order to handle the reusability issue of the catalyst, after separating it via centrifugation, the recovered catalyst was used with 10 mg L^{-1} fresh substrate solutions. All the experimental parameters were kept constant (i.e. [TiO_2] = 500 mg L^{-1}) and the experiments were repeated for 4 sets of each solution. It was found that the photocatalytic efficiency remained sufficiently high after the fourth run yielding comparable values for the substrates conversion during the UV-A photocatalysis (IBP: 61–65%; DCF: 18–21%).

3.2. Identification of the main TPs of IBP and DCF by UPLC/ESI–QToF–MS

Structural elucidation and interpretation of the fragmentation pathways of IBP and DCF and their detected TPs in aqueous solutions, were acquired by using a hybrid mass analyzer QqToF in the ESI(−) and ESI(+) mode, respectively. The analyses generated a large amount of information (experimental and calculated masses of the molecular and fragment ions, relative mass errors, double bond equivalents (DBEs), and proposed elemental compositions of the TPs obtained under optimized conditions of collision energy), reported in Table 2 (for IBP) and Table 3 (for DCF). Most of the accurate mass results were found with an error of less than 2.5 mDa, thus providing a high degree of certainty in the assignment of formulas.

3.2.1. Transformation of IBP

During the application of TiO_2 photocatalysis under UV-A, simulated solar and ultrasound irradiation, numerous TPs were formed since $HO^{\bullet}$ does not exhibit selectivity towards various functional groups, while other reactive species (e.g. $O_2^{\bullet -}$, h^+, e^-) participate in multiple oxido-reductive pathways [47]. The screening of the treated samples in (−)ESI scan mode allowed to tentatively identify the formation of seven TPs. The results indicate that all the tested treatment processes (photocatalysis under UV-A or simulated solar irradiation and sonophotocatalysis) led to the formation of the same products including among others substituted phenols and aromatic carboxylic acids. All of the identified TPs, except two (**TP2** and **TP3**), were eluted before the main peak of IBP at t_R = 4.75 min, indicating the formation of smaller and more polar products when compared to the parent compound. The (−)ESI–MS/MS product ion spectra and putative assignments of characteristic fragment ions of IBP (*m/z* 205.1212) are depicted in Fig. 1(a). The collision-induced-dissociation experiments revealed the formation of only one characteristic fragment ion at *m/z* 161.1311, as a consequence of the typical loss of CO_2 (44 Da).

TP1, eluting at t_R = 4.53 min, yielded a *m/z* ratio of 221.1183 with an error smaller than 2.5 ppm for the formula $C_{13}H_{17}O_3$, which is consistent with the mono-hydroxylated product of IBP. The spectra (MS^2 fragmentation of the molecular ion ($[M-H]^-$ 221) showed decarboxylation to *m/z* 177.1274 (data not shown). Although more isomers could be expected taking into account the free sites in the IBP molecule, in general, there are two principal options for this structural feature, either hydroxylation either on the methylpropyl moiety or hydroxylation on the phenylcarboxylic moiety. Based on the MS^2 experiments, it can be concluded that hydroxylation takes place exclusively on the aromatic ring. This is also supported by the key fragment at *m/z* 93.034 which indicates that methylpropyl and carboxylic moieties of the IBP structure were remained intact. The accurate mass of this fragment ion (*m/z* 93.034) gave a unique elemental composition of C_6H_5O (error −0.4 ppm). A second evidence derives from the presence of strong signal with accurate mass of 119.0506 (C_8H_7O/7.6 ppm) which can be easily assigned to elimination of isobutane (58 Da) and CO_2 (44 Da) group from the molecular ion (**TP1**). Several hydroxylated products of IBP have been detected in sewage [48,49] and in river water (<0.001 μg L^{-1}) [50]. In addition, the hydroxylated-IBP products have been reported to be generated during the photo-Fenton and heterogeneous TiO_2 process under solar artificial irradiation [17,18]. It should be noted that hydroxy-IBP isomers have been also detected as biotransformation-TPs (bio-TPs) of IBP. Quintana et al. [51] detected two isomers of hydroxy-IBP (1′-OH-IBP and

Table 2
Accurate mass measurements of the TPs of IBP as determined by UPLC-(−)ESI–QqToF–MS. Data for (pseudo)-molecular ions correspond to acquisitions in full-scan mode, those of fragment ions to product ion spectra of the protonated molecules.

Compound	t_R (min)	Elemental formula	Mass (*m/z*)		Error		
			Theoretical	Experimental	mDa	ppm	DBE*
IBP	4.75	$C_{13}H_{17}O_2$	205.1229	205.1212	−1.7	−8.3	5.5
		$C_{12}H_{17}$	161.1332	161.1311	−1.9	−11.8	4.5
TP1	4.53	$C_{13}H_{17}O_3$	221.1178	221.1183	0.5	2.4	5.5
		$C_{12}H_{17}O$	177.1279	177.1274	−0.5	−3.1	4.5
		$C_{11}H_{14}O$	162.1045	162.1033	−1.2	−7.2	5
		$C_{10}H_{11}O$	147.081	147.0817	0.7	4.8	5.5
		$C_9H_{10}O$	134.0732	134.0719	−1.3	−9.4	5
		C_9H_8O	132.0575	132.0542	−3.3	−25.1	6
		$C_7H_6O_2$	122.0368	122.0358	−1	−8	5
		C_8H_7O	119.0497	119.0506	0.9	7.6	5.5
		C_6H_5O	93.034	93.034	0	−0.4	4.5
TP2	4.83	$C_{12}H_{15}O_2$	191.1061	191.1072	−1.1	−5.8	5.5
		$C_{12}H_{15}O$	175.1073	175.1123	−5.0	−28.5	5.5
		$C_9H_8O_2$	148.0513	148.0524	−1.1	−7.6	6
		C_7H_5O	105.0333	105.034	−0.7	−6.7	5.5
TP3	4.95	$C_{12}H_{15}O_3$	207.101	207.1021	−1.1	−5.4	5.5
		$C_{11}H_{11}O_3$	191.0697	191.0708	−1.1	−5.9	6.5
		$C_9H_8O_3$	164.0500	164.0473	2.7	16.2	6
		$C_8H_6O_3$	150.0306	150.0317	−1.1	−7.3	6
		$C_8H_7O_2$	135.0453	135.0446	0.7	5.1	5.5
		$C_7H_5O_2$	121.0293	121.029	0.3	2.9	5.5
		C_7H_6O	106.0453	106.0419	3.4	32.4	5
		C_6H_5O	93.0329	93.034	−1.1	−12.3	4.5
TP4	3.14	$C_{12}H_{17}O$	177.1284	177.1279	0.5	2.6	4.5
		$C_{11}H_{14}O$	162.1059	162.1045	1.4	8.9	5
		$C_9H_{10}O$	134.0726	134.0732	−0.6	−4.5	5
		C_9H_8O	132.0568	132.0575	−0.7	−5.4	6
		C_8H_7O	119.0492	119.0497	−0.5	−4.1	5.5
TP5	2.45	$C_{12}H_{15}O$	175.1108	175.1123	−1.5	−8.6	5.5
		$C_{12}H_{13}O$	173.095	173.0966	−1.6	−9.2	6.5
		$C_{12}H_{11}O$	171.0815	171.081	0.5	2.9	7.5
		$C_{11}H_8O$	156.0575	156.0575	0	0	8
		$C_{10}H_{11}O$	147.0814	147.081	0.4	2.8	5.5
		C_8H_7	103.0551	103.0548	0.3	3.2	5.5
TP6	3.03	C_9H_9O	133.0648	133.0653	−0.5	−3.8	5.5
		C_9H_7O	131.0489	131.0497	−0.8	−6.1	6.5
		C_7H_5O	105.0355	105.034	1.5	14.3	5.5
		C_8H_7	103.0549	103.0548	0.1	1	5.5
TP7	3.97	$C_9H_9O_2$	149.0605	149.0603	0.2	1.3	5.5
		$C_8H_6O_2$	134.0365	134.0368	−0.3	−2.1	6
		C_8H_7O	119.0487	119.0497	−1.0	−8.3	5.5

* DBE = Double bond equivalent.

2′-OH-IBP) as the main bio-TPs of IBP during laboratory biodegradation tests, where 2′-OH-IBP was generated before 1′-OH-IBP and both were degraded or disappeared quickly from the bioreactor. Hydroxy-IBP (2′-OH-IBP) was also identified in biodegradation experiments under oxic conditions with activated sludge in both biofilm and batch reactor [52]. Laboratory studies indicated that hydroxy-IBP was identified and readily degraded in a river biofilm reactor [11]. In addition, 1′-OH-IBP and 2′-OH-IBP were monitored quantitatively along the biodegradation processes occurring in different batch activated sludge experiments [53]. During the very early stages of IBP degradation by the white-rot fungi *T. Versicolor*, 1′-OH-IBP and 2′-OH-IBP were detected, while these metabolites were subsequently degraded to 1,2 di-hydroxy-IBP [28].

The ESI–MS^2 spectra patterns of **TP2** (*m/z* 191.1072) is consistent with 4-(1-carboxyethyl) benzoic acid indicating the fact that direct demethylation took place in parallel reaction with the hydroxylation process. The spectrum is characterized by the fragment ion at *m/z* 148.0524 that arises from the typical loss of C_3H_7.

The next TP identified provided a molecular ion at *m/z* 207.1021 (**TP3**). Based on the best-fit formula of $C_{12}H_{15}O_3$ and the mass difference of 16 Da compared to the **TP2**, the elemental composition may be rationalized by the formation of hydroxyl-demethylated IBP derivative. The loss of 43 Da, for the elimination of isopropyl radical, led to the appearance of the highest mass ion at *m/z* 164.0473, which with further loss of methyl group resulted in the *m/z* 150.0317 fragment ion.

Decarboxylation of **TP1** led to the formation of **TP4** with *m/z* 177.1279 molecular ion. The spectrum is characterized by the fragment ion at *m/z* 119.0497 that arises from the loss of isobutane moiety. **TP4** has been also identified as major TP during the photo-Fenton process [17] and photocatalytic TiO_2 degradation of IBP [18] as well as under gamma irradiation process [54].

The next TP identified provided a molecular ion at *m/z* 175.1123 (**TP5**). Based on the best-fit formula of $C_{12}H_{15}O^-$ and the mass difference of 2 Da compared to **TP4**, the elemental composition may be rationalized by the formation of keto-derivative. Based on the MS^2 spectrum of this product that shows the presence of a characteristic fragment ion at *m/z* 147.081 corresponding to the loss of ethene, which with further cleavage of CH_2CHO moiety and hydrogen abstraction resulted in the *m/z* 103.0548 fragment

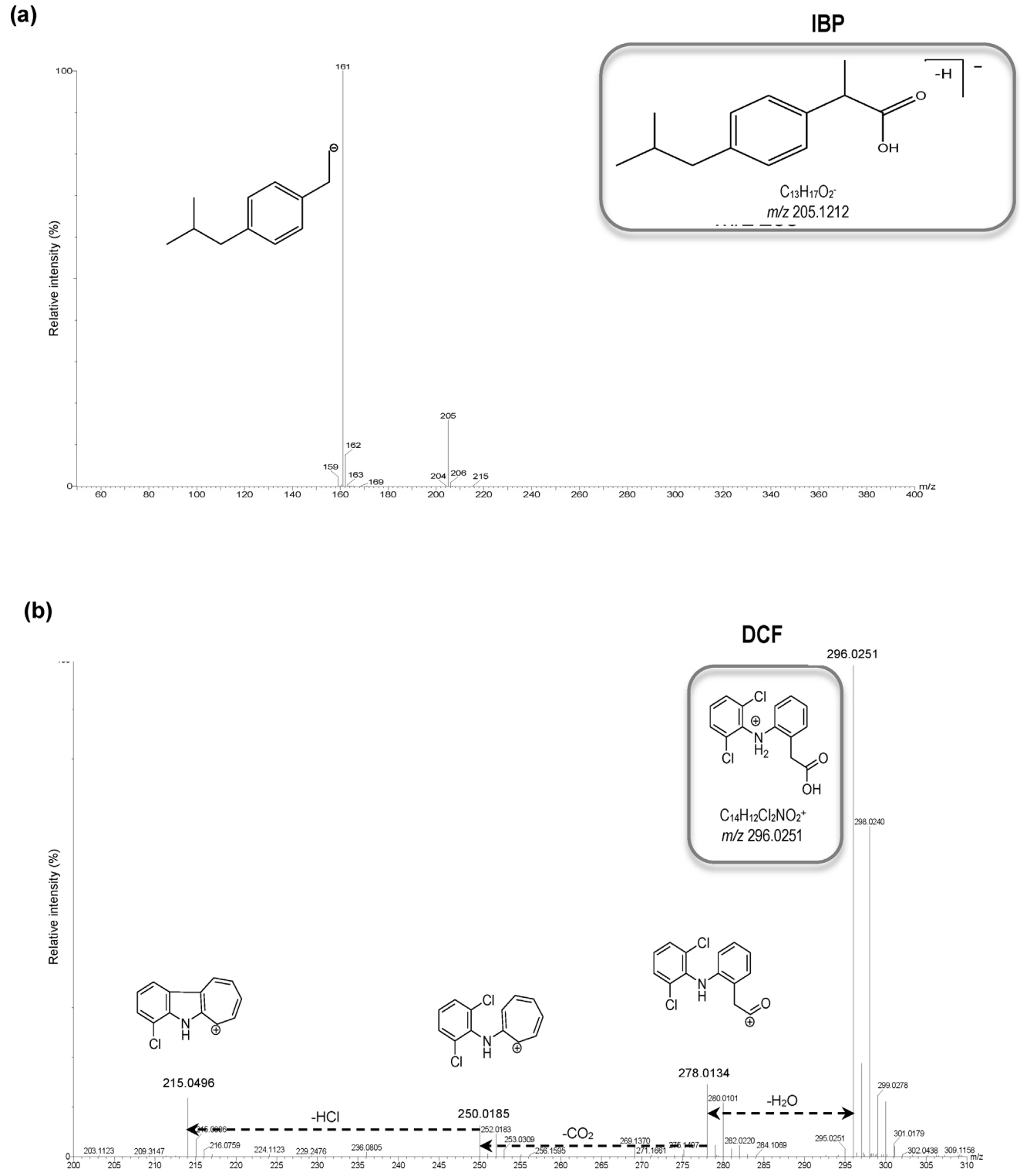

Fig. 1. Spectra obtained in ESI(±)-MS^2 experiments at QqToF instrument for IBP and DCF and proposed fragmentation patterns.

ion, the structure of 4-isobutylacetophenone would be proposed as more predominated. Its formation has been also reported as the main TP during the photo-Fenton [18], photocatalytic (Fe^{3+}, TiO_2), sonolytic and sonophotocatalytic [25] degradation of IBP. Furthermore, Caviglioli et al. [55], observed its formation during the oxidative degradation of IBP using permanganate solution.

The product with the *m/z* 133.0653 may correspond to 4-ethylbenzaldehyde (**TP6**). The loss of 28 Da, typical for CO group led to the appearance of the fragment ion at *m/z* 105.034. The strong signals observed at *m/z* 131.0497 and *m/z* 103.0548 would be attributed to the intramolecular cyclization of the **TP6**, as presented in Scheme 1. **TP6** has been also reported as main TP of IBP by the photoelectron-Fenton [56], photo-Fenton [18], photocatalytic [17,25], sonolytic and sonophotocatalytic [25] degradation of IBP, thermal and oxidative treatment ($KMnO_4$, H_2O_2 and $K_2Cr_2O_7$) as well as by gamma irradiation process [54].

Table 3
Accurate mass measurements of the TPs of DCF as determined by UPLC–(+)ESI–QqToF–MS. Data for (pseudo)-molecular ions correspond to acquisitions in full-scan mode, those of fragment ions to product ion spectra of the protonated molecules.

Compound	t_R (min)	Elemental Formula	Error Mass (*m/z*)		Error		
			Theoretical	Experimental	mDa	ppm	DBE*
DCF	3.83	$C_{14}H_{12}Cl_2NO_2$	296.0245	296.0251	0.6	2.0	8.5
		$C_{14}H_{10}Cl_2NO$	278.0139	278.0134	0.5	2.5	8.5
		$C_{13}H_{10}Cl_2N$	250.0190	250.0185	1.2	−1.6	8.0
		$C_{13}H_{10}ClN$	215.0502	215.0496	0.8	−3.7	7.5
		$C_{13}H_{10}N$	180.0813	180.0808	1.0	1.0	7.5
TP*1 (A) and (B)	3.82	$C_{14}H_{11}Cl_2NO_3$	311.0116	312.0117	0.3	1.0	8.5
		$C_{14}H_{10}Cl_2NO_2$	294.0083	294.0089	0.5	2.1	8.0
		$C_{13}H_{10}Cl_2NO$	266.0134	266.0165	0.6	−0.5	8.5
		$C_{13}H_{10}ClNO$	231.0445	231.0478	1.5	−1.2	7.0
		$C_{13}H_{10}NO$	196.0757	196.0793	0.4	−2.4	6.0
TP*2 (A) and (B)	3.41	$C_{14}H_{12}Cl_2NO_4$	328.0138	328.0464	2.4	7.3	8.5
		$C_{14}H_{10}Cl_2NO_3$	310.0032	309.9882	−1.6	−4.9	8.5
		$C_{13}H_{10}Cl_2NO_2$	282.0083	282.0157	1.0	2.5	9.0
		$C_{13}H_{10}ClNO_2$	247.0395	247.0546	−2.3	−2.4	8.5
		$C_{13}H_{10}NO_2$	212.0706	212.0385	0.2	0.9	8.0
TP*3 (A) and (B)	3.86	$C_{13}H_{10}Cl_2NO$	266.0167	266.0139	2.8	10.5	8.5
		$C_{13}H_{10}ClNO$	231.0445	231.0451	−1.9	−8.2	9.0
TP*4	4.44	$C_{13}H_{10}NO_2Cl_2$	282.0062	282.0083	−2.7	−9.6	8.5
TP*5	4.49	$C_{13}H_8Cl_2NO_2$	280.0013	280.0052	−3.5	−0.5	8.5
		$C_{12}H_8Cl_2NO$	251.9977	252.0199	1.6	1.2	8.5
		$C_{12}H_8ClNO$	217.0289	217.0420	−2.1	−2.8	9.0
TP*6	4.49	$C_{14}H_{10}Cl_2NO_2$	293.7869	293.9630	1.3	2.6	8.0
		$C_{13}H_{10}Cl_2NO$	266.0134	265.9824	1.0	1.8	8.0
		$C_{13}H_{10}ClNO$	231.0445	231.0224	−1.2	0.8	7.0
		$C_{13}H_9NO$	195.0679	195.3815	0.5	1.7	7.0
TP*7	3.02	$C_6H_5Cl_2NO$	177.9825	177.9826	−0.1	−0.6	8.5
		C_6H_6ClNO	143.0132	143.0130	0.8	2.3	8.5

* DBE = Double bond equivalent.

Finally, the structure of **TP7** molecular ion at *m/z* 149.0603 was proposed as a consequence of cleavage of isobutyl moiety from the primary molecule (*m/z* 205.1212). The loss of 15 Da typical for methyl group resulted in fragment ion at *m/z* 134.0368. To the best of our knowledge this compound was the only one from the aforementioned TPs that have been identified by adopting photocatalytic and sonophotocatalytic processes and has not been found with *in vivo* metabolic experiments and other advanced oxidation studies.

3.2.2. Transformation of DCF

The screening of the treated samples in (+)ESI scan mode allowed confirming the formation of ten TPs with retention times shorter than that of the parent compound (Table 3). In most cases, TPs were easily recognizable by the presence in the mass spectrum, of the resolved isotopic cluster characteristic of compounds that contain chlorine atoms in their molecules. Some of the identified TPs, have already been reported by other authors as the main TPs of DCF during photolysis [19,57,58], ozonation [22,23], electrooxidation [59], heterogeneous photocatalysis [16,60], and sonolysis [24].

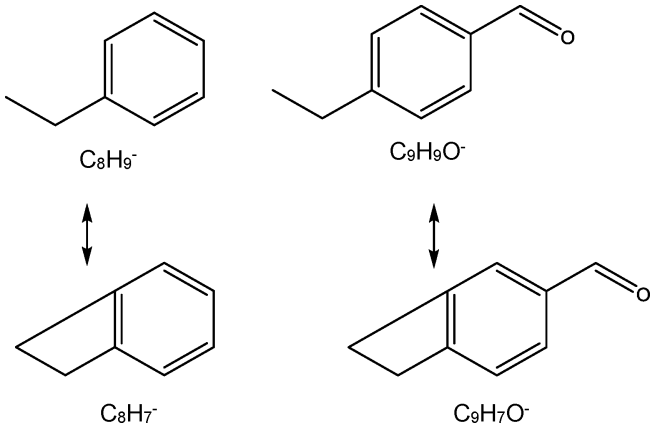

Scheme 1. Intramolecular cyclization of **TP6** (*m/z* 133.0653).

Fig. 1(b) shows the mass spectrum of DCF that exhibited a molecular ion peak at *m/z* 296.0251. The product ion profile of the protonated molecule derives from the sequential loss of H_2O (*m/z* 278.0134) and CO (*m/z* 250.0185) followed by cleavage of the chlorine atoms as radicals (*m/z* 215.0496 and 180.0808), which was corroborated through pseudo-MS^3 experiments by selecting the corresponding fragment ions.

The formation of hydroxylated derivatives of DCF (**TP*1 (A)** and **(B)**) was confirmed by the presence of compounds whose formula showed an increase by one oxygen atom with respect to the formula of DCF, without any alterations in the DBE. These TPs yielded an accurate mass of 312.0117 ($C_{14}H_{11}Cl_2NO_3$), which is consistent with the mono-hydroxylated product of DCF, named as 4′-hydroxy DCF (4′-OH-DCF) and 5′-hydroxy DCF (5′-OH-DCF) confirmed by authentic standards, respectively. 4′-OH-DCF (and to a minor extent 5′-OH-DCF) are the major metabolites of the oxidative DCF metabolism in humans, which is catalyzed by different types of cytochromes in the human liver. The 4′-OH-DCF metabolite is produced by the cytochrome P-450 isoenzyme CYP2C9 [61], whereas 5-hydroxylation of the more electron-rich aromatic ring of the drug is catalysed by several cytochromes [62]. The two spectra (MS^2 fragmentation of the molecular ion $[M+H]^+$ 312.0117) were almost identical and rendered intense signal at *m/z* 294.0089 corresponding to the loss of water, which with further loss of CO resulted in the *m/z* 266.0165 fragment ion. The loss of 35 Da, typical

for the elimination of one chlorine atom, led to the appearance of the fragment ion at *m/z* 231.0478, which upon further loss of the second chlorine atom resulted in the *m/z* 196.0793 fragment ion. 4′-OH-DCF and 5′-OH-DCF were among the detected TPs when DCF was irradiated with ultrasound [24,25] and γ-radiolysis [63]. 5′-OH-DCF was also reported as TP under electro-oxidation of DCF [59]. Hydroxy DCF isomers were also detected as TPs under ozonation [53], photo-Fenton [44] as well as under photocatalytic conditions [16,22,60]. In addition, 4′-OH-DCF was identified as the main bio-TP during the microbial degradation test of DCF [64].

With further hydroxyl radical oxidation, di-hydroxylation products (**TP*2 (A)** and **(B)**) were formed (*m/z* increases of 32 Da), which verifies the assumption of hydroxyl substitution, since the hydroxyl group increases the electron density of the aromatic ring and thus, hydroxyl radical electrophilic adductions proceed faster [63]. As in the case of **TP*1**, the product ion spectrum of the di-hydroxy DCF (*m/z* 328.0464) was characterized by stepwise elimination of H_2O (*m/z* 309.9882), CO (*m/z* 282.0157), and two Cl atoms (*m/z* 247.0546 and 212.0385).

The next TP derivatives identified provided a molecular ion at *m/z* 266.0139 (**TP*3 (A)** and **(B)**). Based on the best-fit formula of $C_{13}H_{10}Cl_2NO$ (protonated molecule) a plausible structure corresponded to decarboxylation and dehydrogenation from the hydroxylated DCF derivative (**TP*1**). The ESI–MS^2 spectra of **TP*3** is characterized by a strong signal at *m/z* 231 which corresponds to the loss of one chlorine atom (35 Da).

Further, hydroxylation of **TP*3** resulted in the formation of **TP*4** with an accurate mass of *m/z* 282.0083, which was further transformed to **TP*5**. **TP*4** was previously observed by Soufan et al. [65] during water chlorination. Analogous to mono- and dihydroxy-DCF derivatives, **TP*5** showed the protonated molecule $[M+H]^+$ with *m/z* 280.0052 and the successive elimination of CO and one chlorine atom to form fragment ions at *m/z* 252.0199 and *m/z* 217.0420, respectively. Based on the best-fit formula of $C_{13}H_8NO_2Cl_2$ (protonated molecule) and the mass difference of 2 Da compared to the hydroxylated **TP*4**, the elemental composition may be rationalized by the formation of an aldehyde. The formation of product **TP*5** was observed during the UV oxidation of DCF [21].

The formation of **TP*6** corresponds to a decrease in molecular mass for 18 Da from **TP*1**, suggesting a dehydratation of the hydroxyl-DCF. The MS/MS spectrum of *m/z* 293.9630 showed a neutral loss of CO (28 Da), producing a fragment at *m/z* 265.9824, and a loss of Cl at *m/z* 231.0224.

Finally, the product **TP*7** with a molecular ion *m/z* 177.9826 was assumed, derived from the cleavage of the non-chlorinated ring, after oxidation–hydroxylation, followed by a further decarboxylation step. Based on the presence of the fragment with accurate mass of *m/z* 143.0130 (C_6H_6ClNO, protonated molecule) resulting from the loss of Cl radical, it can be assumed that hydroxylation took place on the chlorinated aromatic ring. This TP has been also proposed by Pérez-Estrada et al. [44] under the degradation of DCF in aqueous solutions by photo-Fenton reaction as well as by Coelho et al. [23] under the degradation of DCF by ozonation.

3.3. Proposed transformation pathway and evolution profile of TPs

Overall, no differences were observed in the nature of TPs formed for each substrate among the experiments performed; photocatalysis under UV-A, and simulated solar irradiation, and

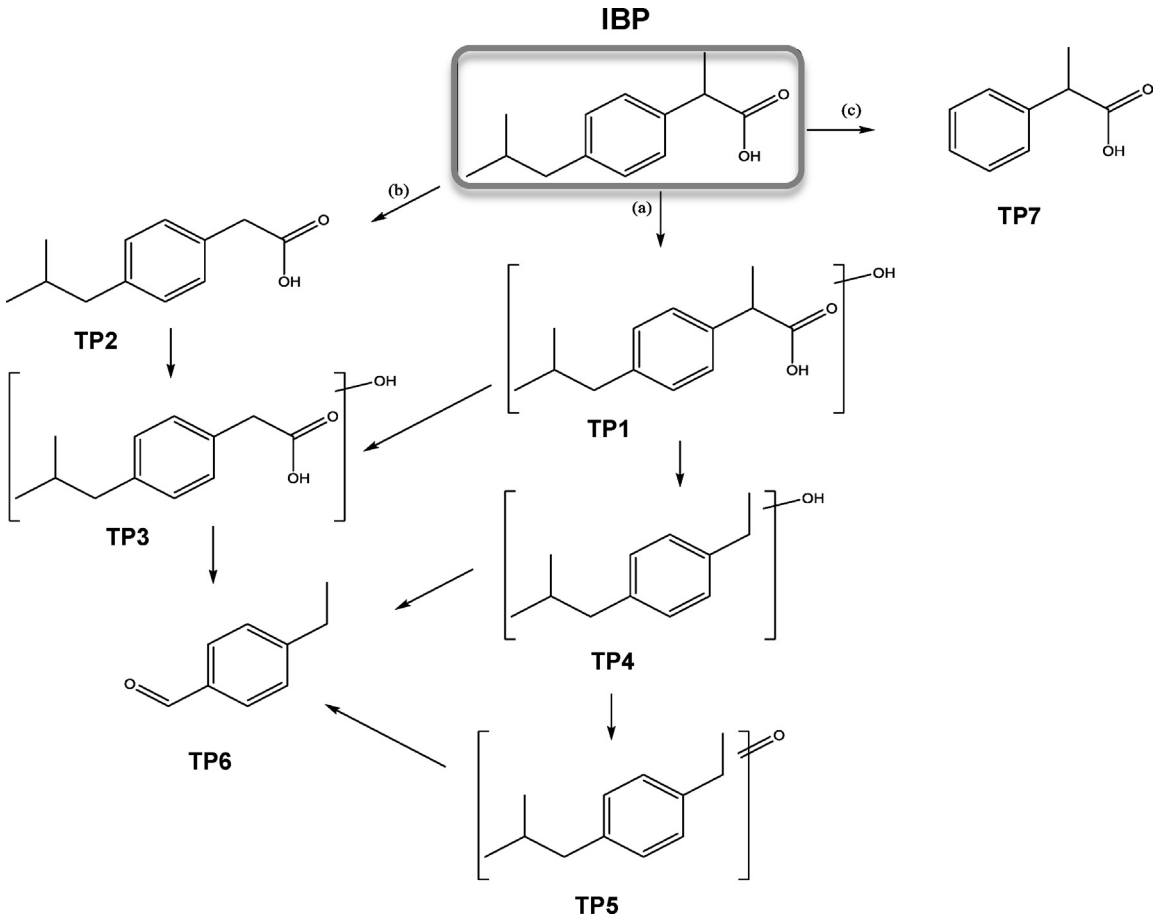

Scheme 2. Tentative transformation pathway of IBP degradation by photocatalysis under UV-A and simulated solar irradiation, and sonophotocatalysis.

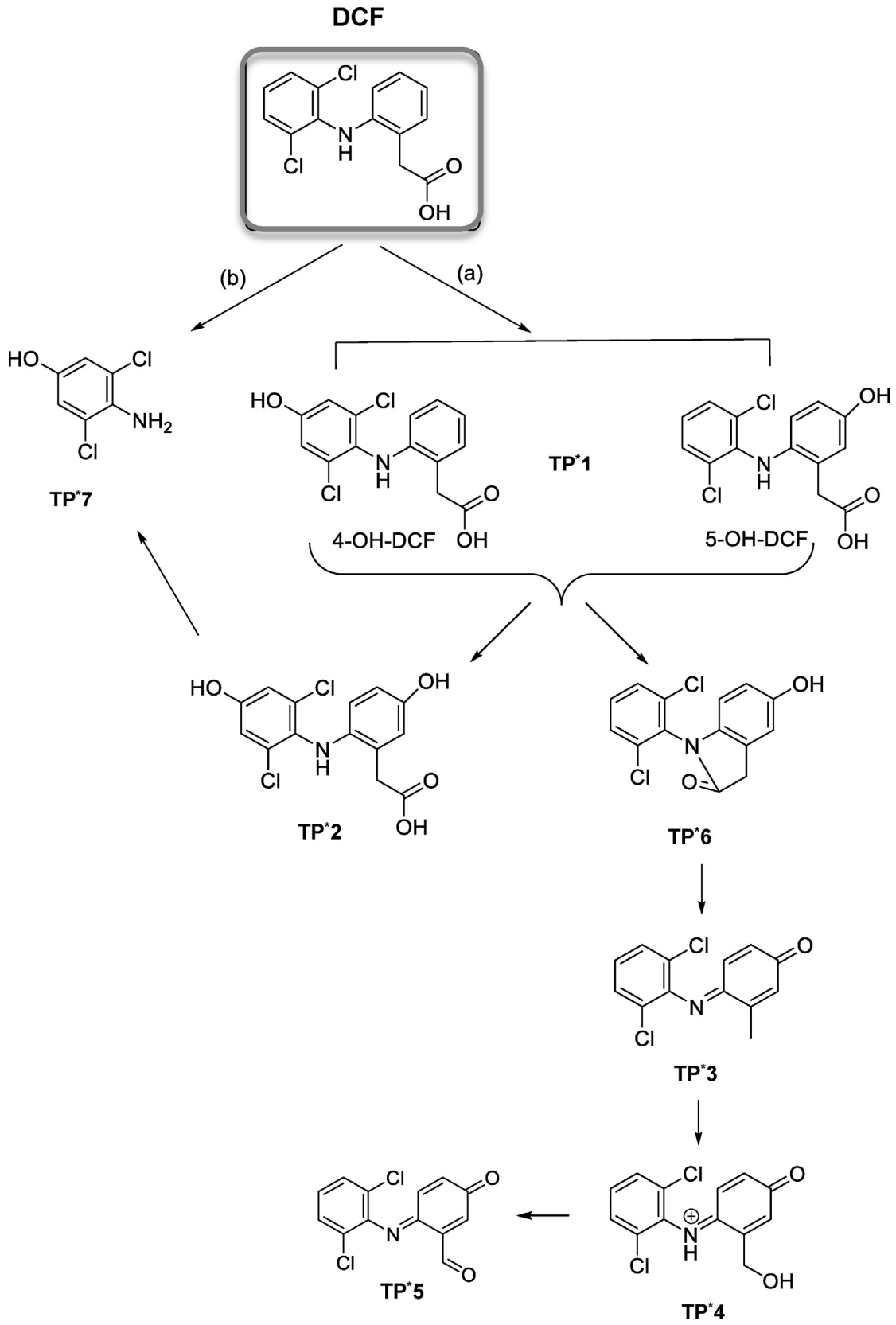

Scheme 3. Tentative transformation pathway of DFC degradation by photocatalysis under UV-A and simulated solar irradiation, and sonophotocatalysis.

sonophotocatalysis, indicating the involvement of similar reaction mechanisms. The formation of the TPs was expressed as the relative intensity measured by integrating the LC–MS peaks of the corresponding TP with that of the parent compound at different treatment times, since due to the lack of authentic analytical standards for the newly identified products their quantitative determination was not possible. Here it is noted that the different intensities of the same TPs observed during the three oxidation processes could be attributed to the different substrates degradation kinetics observed during the oxidation processes.

3.3.1. IBP degradation pathway

On the basis of the results presented herein and previous studies on the IBP oxidation [17,25,55], biodegradation [11,51,52] and metabolism [28,48], three competing pathways (Scheme 2) can be drawn, in which hydroxylation, demethylation, decarboxylation, cleavage of isobutyl moiety, and oxidation of hydroxyl groups are described as major steps during the transformation processes.

In the first pathway, either the methylpropyl or the phenylcarboxylic moiety of the IBP molecule was attacked by HO• to form mono-hydroxylated species (**TP1**). This TP was either further oxidized or induced decarboxylation (**TP4**, **TP5**), which were further transformed to **TP6**. In a parallel reaction pathway, a methyl group of IBP molecule is attacked by HO• to form a demethylated intermediate (**TP2**). The latter underwent the same mechanism, via hydroxylation (**TP3**), oxidation, demethylation and decarboxylation, and finally was transformed to lower molecular weight products. In the third pathway, the transformation proceeded through the detachment of isobutyl group by leading to the formation of 2-phenylpropanoic acid (**TP7**).

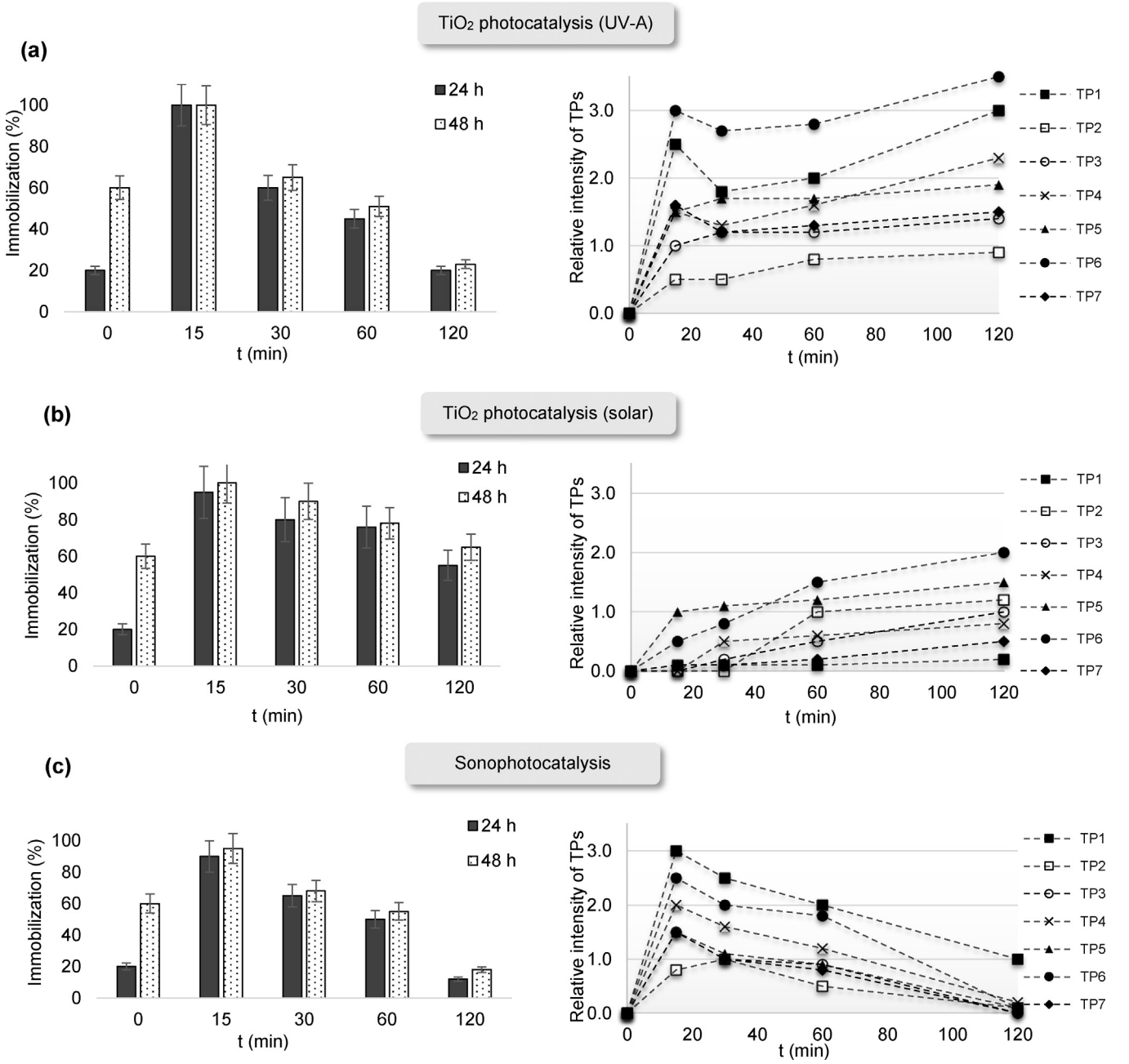

Fig. 2. Evolution of toxicity to *D. magna* after 24 h and 48 h of exposure during: (a) UV-A photocatalysis, (b) photocatalysis under simulated solar irradiation, and (c) sonophotocatalysis. The evolution profile of the main TPs during the degradation of IBP is depicted in each case. Experimental conditions: $[IBP]_0 = 10\ mg\ L^{-1}$; $[TiO_2]_0 = 500\ mg\ L^{-1}$; 9 W UV-A, xenon lamp 1 kW, ultrasound intensity power 8.4 W cm^{-2}, air sparging.

During the heterogeneous photocatalysis of IBP under UV-A irradiation, TPs emerged within the first 15 min of irradiation and remained abundant in the solution until the end of the treatment (120 min), with **TP6** exhibiting the highest relative intensity. Moreover, the results indicate that differences in the TPs formation profile existed when simulated solar irradiation was used (the TPs were formed at lower rate in comparison to the UV-A-driven photocatalysis and detected at lower intensities), probably as a consequence of the slower degradation of the parent compound ($k_{UVA+TiO_2}$ = 24.6 × 10^{-3} min^{-1}; $k_{solar+TiO_2}$ = 8.5 × 10^{-3} min^{-1}). During the sonophotocatalytic experiments, the TPs appeared promptly; after 15 min they reached a concentration maximum before being almost degraded.

3.3.2. DCF degradation pathway

MS analysis suggests that oxidation of DCF, under the investigated experimental conditions, mainly proceeds by oxidation and hydroxylation reactions between chloroaniline and phenylacetic acid (Scheme 3).

Hydroxylation reactions are common in most of the oxidative processes. The addition of the electrophilic HO• to the aromatic ring forms a resonance-stabilized carbon-centered radical with subsequent elimination of hydrogen radical, yielding the mono

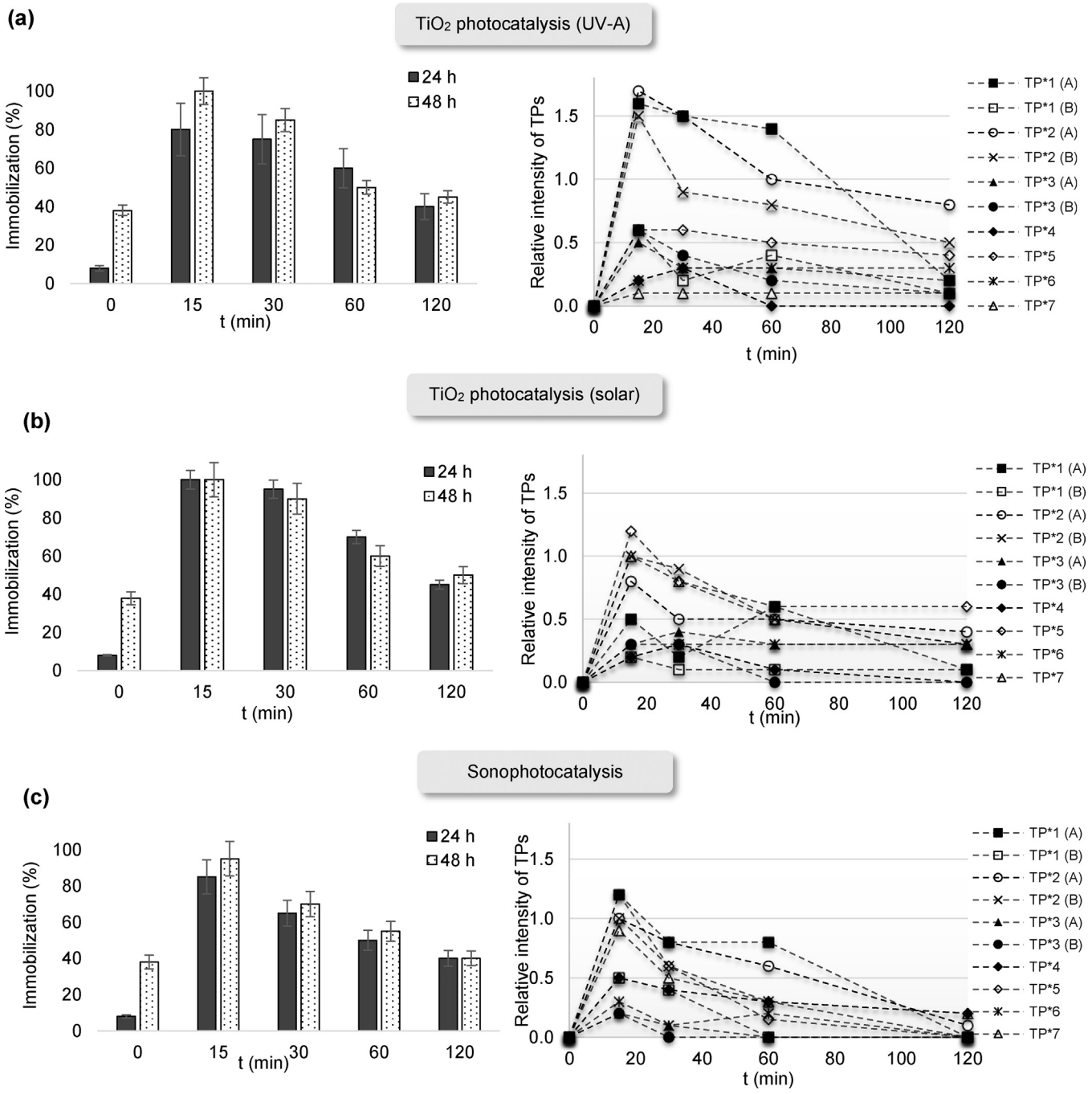

Fig. 3. Evolution of toxicity to *D. magna* after 24 h and 48 h of exposure during: (a) UV-A photocatalysis, (b) photocatalysis under simulated solar irradiation, and (c) sonophotocatalysis. The evolution profile of the main TPs during the degradation of DCF is depicted in each case. Experimental conditions: $[DCF]_0$ = 10 mg L^{-1}; $[TiO_2]_0$ = 500 mg L^{-1}; 9 W UV-A, xenon lamp 1 kW, ultrasound intensity power 8.4 W cm^{-2}, air sparging.

hydroxylated species (4′-OH-DCF, 5′-OH-DCF) as the first step in the DCF degradation. Generally, the specificity of the electrophilic aromatic substitution is typically governed by the nature of the substitute, which may account for our observation of two different products with the same *m/z* ratio. The aforementioned TPs were either further oxidized (**TP*2 (A)** and **(B)**, **TP*6**) and/or induced the loss of the carboxylic moiety leading to the formation of decarboxylated derivative (**TP*3**), which was further transformed to **TP*4** and **TP*5**. The formation of **TP*7** also indicates the cleavage of the C–N bond of DCF as a preferential route, which has been originated from a series of C–N cleavage products such as the formation of 2,6-dichlorophenol and 4-chlorocathecol, while cathecol and hydroquinone are probably formed from the other aromatic ring, through the loss of the side chain [16].

During the UV-A and solar-driven photocatalytic experiments, a similar profile of the formation of TPs was observed, where **TP*1** (4′-OH-DCF and 5′-OH-DCF) and **TP*2** were mainly detected at higher relative intensities and higher reaction times compared to the other TPs. An important observation made during these experiments was that the hydroxylated-DCF species remained in the solution until 120 min; however, 5′-OH-DCF appeared at much lower abundance compared to 4′-OH-DCF. Under the combined action of ultrasound and UV-A irradiation in the presence of TiO_2, the TPs were detected at the maximum concentration in the first 15 min (**TP*1** and **TP*2** were the most abundant) and most of them disappeared completely by the end of the treatment.

3.4. Ecotoxicity assessment

The acute toxicity of the treated solutions to *D. magna* was monitored as a function of the treatment and exposure time during the examined treatment processes (Figs. 2 and 3). The immobilization of the species was monitored after 24 h and 48 h of exposure to the tested samples. In the same Figures (on their right side), the plots of the peak intensities recorded in the LC-TOF/MS profiles for the main TPs generated during the experiments against the irradiation time are shown.

The untreated IBP solution (10 mg L^{-1}) was found to be moderately toxic to *D. magna* inducing an immobilization of 20% and 60% after 24 h and 48 h of exposure, respectively. During the application of the photocatalytic process in the presence of UV-A, solar and ultrasound irradiation, a change in the immobilization of *D. magna* was observed indicating that the produced oxidation products are characterized by different toxicity.

A similar toxicity profile was observed during the treatment of IBP solution with UV-A photocatalysis and sonophotocatalysis. The toxicity of the treated samples taken after 15 min (24 h and 48 h of exposure), dramatically increased to approximately 100%. This is in accordance with the fact that at this treatment time, the TPs were detected at higher relative abundances (especially **TP6** which was detected at higher intensity). From that time onwards, a gradual decrease in *D. magna* immobilization to 20% was observed until the end of the treatment as toxic intermediates were degraded further. Under the simulated solar irradiation conditions, the acute toxicity of IBP solution to *D. magna* was generally very high over the time-course of the process and, especially during the final stages, a fact that can be possibly attributed to the slower degradation kinetics (immobilization > 70%).

Untreated DCF solutions displayed a slight toxicity on *D. magna* after 24 h of exposure (less than 10%) that was increased to 38% after 48 h of exposure. The initial toxicity increased rapidly up to 80% (24 h) and 100% (48 h) after 15 min of irradiation indicating that compounds more toxic than the parent compound were formed (Fig. 3). This also may be attributed to the formation of a variety of chloroderivatives whose toxicity has been demonstrated to be very high [66]. It is worth mentioning that the highest toxicity observed is in accordance with the maximum concentration of the TPs formed. From 30 min to 120 min of irradiation the immobilization decreases, remaining however still high at values above 50%. At this time, the TPs formed were still present in the solution, while synergistic effects among them may also be considered.

In general, the alterations in the immobilization of daphnids can be attributed to a concomitant generation of various TPs during the oxidation of the parent compounds which can exhibit individual or/and synergistic toxic effects [67]. Due to the large number of TPs generated, it is difficult to impose which of them was responsible for the substantial increase of toxicity. Based on the available scientific literature [68,69] **TP5** exhibits a toxic effect because it has a lytic activity on erythrocytes. In addition, **TP4** was also found to exert toxic effect by measuring the amount of cell protein and intracellular enzymatic activity of lactic dehydrogenase (LDH) and transaminase (GOT) in cultured fibroblasts [68]. Dystrophic lesions affecting the liver, kidney, and skin have been reported to occur by **TP6** using zebrafish (*Danio rerio*) as the test microorganism [70].

A similar trend in the toxicity of DCF treated solutions was observed by Rizzo et al. [71] and Calza et al. [16] who investigated the toxicity of the photocatalytically treated DCF (2.5 mg L^{-1}; 15 mg L^{-1}) aqueous solutions to *D. magna*. Schmitt-Jansen et al. [57] investigated the phytotoxicity of DCF aqueous solutions (50 mg L^{-1}) exposed to natural sunlight using synchronized cultures of the unicellular chlorophyte *S. vacuolatus*. The time course of the relative concentration of three TPs significantly correlated with enhanced phytotoxicity during the experiments.

4. Conclusions

In this work, kinetic and mechanistic aspects of the degradation of IBP and DCF were investigated to appraise the behaviour of these compounds during the application of (sono)photocatalytic processes. From a kinetic point of view, the degradation of the substrates can be modeled by a pseudo first-order rate expression, while the apparent first-order rate constant was found to increase in the following order: Sonolysis (US) ≈ sonocatalysis < photocatalysis (UV-A and simulated solar irradiation) < sonophotocatalysis. The beneficial synergy of process integration, UV-A driven TiO_2-photocatalysis and sonolysis (sonophotocatalysis), may be attributed to the increased production of reactive free radicals as well as enhanced catalytic activity.

Even though differences with respect to the apparent rate constants were observed among the oxidation processes applied for each substrate, the fact that the same TPs were detected in the different experiments indicate similar reaction mechanisms during the treatments. The screening of the treated samples in (±) ESI scan mode allowed to tentatively identify the formation of seven TPs of IBP and ten TPs of DCF under UV-A and simulated solar irradiation photocatalysis and sonophotocatalysis. Some of the identified TPs match those found in biodegradation and advanced oxidation studies, while several new species have been found additionally. In some cases, the identification of more than one isomer was the consequence of the non-selectivity of the $HO^{\bullet}$ attack. The degradation pathway of IBP includes mainly decarboxylation, demethylation and hydroxylation reactions, while the oxidation of DCF, mainly proceeded by oxidation and hydroxylation reactions between chloroaniline and phenylacetic acid. In some cases, cleavage of the aromatic rings occurred leading to the formation of TPs with lower molecular mass.

The treated samples displayed a varying toxicity profile for each parent compound which can be attributed to their associated TP toxic effects. UV-A photocatalysis and sonophotocatalysis were able to achieve a reduction of the toxicity of the treated IBP solution.

This decrease was more pronounced in the case of sonophotocatalysis where the toxicity of IBP aqueous solution was significantly decreased to 20% after 48 h of exposure. Nevertheless, the acute toxicity of IBP aqueous solution towards *D. magna* increased over the time-course of the solar-driven photocatalytic experiments. A similar toxicity profile was observed during the treatment of DCF aqueous solution with the advanced chemical processes used herein. Although the immobilization decreased throughout the processes, it still remained higher than that observed for the DCF untreated solutions (> 50%).

Acknowledgements

This work was co-funded by the Republic of Cyprus and the European Regional Development Fund through grants UPGRADING/DURABLE/0308/07 (Project title: **IX-Aqua)** and "Nireas-IWRC" (ΝΕΑΥΠΟΔΟΜΗ/ΣΤΡΑΤΗ/0308/09) through the Research Promotion Foundation of Cyprus. Sandra Pérez acknowledges the contract from the Ramón y Cajal Program of the Spanish Ministry of Economy and Competitiveness. The studies have partly been supported by the Spanish Ministry of Economy and Competitiveness [64551/HID and Consolider-Ingenio 2010 Scarce CSD2009-00065].

References

[1] P.H. Roberts, K.V. Thomas, Sci. Total Environ. 356 (2006) 143–153.
[2] R. Szabó, C. Megyeri, E. Illés, K. Gajda-Schrantz, P. Mazellier, A. Dombi, Chemosphere 84 (2011) 1658–1663.
[3] K. Kümmerer, Chemosphere 45 (2001) 957–969.
[4] M. Carballa, F. Omil, J.M. Lema, M. Llompart, C. Garcı′a-Jares, I. Rodrı′guez, M. Gómez, T. Ternes, Water Res. 38 (2004) 2918–2926.
[5] M. Clara, B. Strenn, O. Gans, E. Martinez, N. Kreuzinger, H. Kroiss, Water Res. 39 (2005) 4797–4807.
[6] A.L. Spongberg, J.D. Witter, Sci. Total Environ. 397 (2008) 148–157.
[7] S. Pérez, D. Barceló, Trends Anal. Chem. 27 (2008) 836–846.
[8] G.R. Boyd, H. Reemtsma, D.A. Grimm, S. Mitra, Sci. Total Environ. 311 (2003) 135–149.
[9] I. Muñoz, J.C. López-Doval, M. Ricart, M. Villagrasa, R. Brix, A. Geiszinger, A. Ginebreda, H. Guasch, M. de Alda, A.M. Romaní, Environ. Toxicol. Chem. 28 (2009) 2706–2714.
[10] D.W. Kolpin, E.T. Furlong, M.T. Meyer, E.M. Thurman, S.D. Zaugg, L.R. Barber, H.T. Buxton, Environ. Sci. Technol. 36 (2002) 1202–1211.
[11] M. Winkler, J.R. Lawrence, T.R. Neu, Water Res. 35 (2001) 3197–3205.
[12] M. Petrović, M.D. Hernando, M.S. Díaz-Cruz, D. Barceló, J. Chromatogr. A 1067 (2005) 1–14.
[13] A. Nikolaou, S. Meric, D. Fatta, Anal. Bioanal. Chem. 387 (2007) 1225–1234.
[14] I. Michael, L. Rizzo, C. McArdell, C. Manaia, C. Merlin, T. Schwartz, C. Dagot, D. Fatta-Kassinos, Water Res. (2012).
[15] Z. Frontistis, D. Mantzavinos, Ultrason. Sonochem. 19 (2012) 77–84.
[16] P. Calza, V. Sakkas, C. Medana, C. Baiocchi, A. Dimou, E. Pelizzetti, T. Albanis, Appl. Catal., B: Environ. 67 (2006) 197–205.
[17] F. Méndez-Arriaga, S. Esplugas, J. Giménez, Water Res. 42 (2008) 585–594.
[18] F. Méndez-Arriaga, S. Esplugas, J. Gimenez, Water Res. 44 (2010) 589–595.
[19] A. Agüera, L. Perez Estrada, I. Ferrer, E. Thurman, S. Malato, A. Fernández-Alba, J. Mass Spectrom. 40 (2005) 908–915.
[20] P. Bartels, W. von Tümpling, Sci. Total Environ. 374 (2007) 143–155.
[21] R. Salgado, V. Pereira, G. Carvalho, R. Soeiro, V. Gaffney, C. Almeida, V.V. Cardoso, E. Ferreira, M. Benoliel, T. Ternes, J. Hazard. Mater. 244-245 (2013) 516–527.
[22] D. Vogna, R. Marotta, A. Napolitano, R. Andreozzi, M. d'Ischia, Water Res. 38 (2004) 414–422.
[23] A.D. Coelho, C. Sans, A. Agüera, M.J. Gómez, S. Esplugas, M. Dezotti, Sci. Total Environ. 407 (2009) 3572–3578.
[24] J. Hartmann, P. Bartels, U. Mau, M. Witter, W. Tümpling, J. Hofmann, E. Nietzschmann, Chemosphere 70 (2008) 453–461.
[25] J. Madhavan, F. Grieser, M. Ashokkumar, J. Hazard. Mater. 178 (2010) 202–208.
[26] F. Pomati, S. Castiglioni, E. Zuccato, R. Fanelli, D. Vigetti, C. Rossetti, D. Calamari, Environ. Sci. Technol. 40 (2006) 2442–2447.
[27] S. Schnell, N.C. Bols, C. Barata, C. Porte, Aquat. Toxicol. 93 (2009) 244–252.
[28] E. Marco-Urrea, M. Pérez-Trujillo, T. Vicent, G. Caminal, Chemosphere 74 (2009) 765–772.
[29] J.L. Oaks, M. Gilbert, M.Z. Virani, R.T. Watson, C.U. Meteyer, B.A. Rideout, H. Shivaprasad, S. Ahmed, M.J.I. Chaudhry, M. Arshad, Nature 427 (2004) 630–633.
[30] M.D. Hernando, M. Mezcua, A. Fernández-Alba, D. Barceló, Talanta 69 (2006) 334–342.
[31] J. Schwaiger, H. Ferling, U. Mallow, H. Wintermayr, R. Negele, Aquat. Toxicol. 68 (2004) 141–150.
[32] R. Triebskorn, H. Casper, A. Heyd, R. Eikemper, H. Köhler, J. Schwaiger, Aquat. Toxicol. 68 (2004) 151–166.
[33] Directive 2000/60/EC of the European Parliament and of the Council of 23 October 2000 establishing a framework for Community action in the field of water policy (OJL 327, 22.12.2000, P. 1) ⟨http://eurlex.europa.eu/LexUriServ/LexUriServ.do?uri=CELEX:02000L0060-20090113:EN:NOT⟩.
[34] COM, Proposal for a Directive of the European Parliament and of the Council amending Directives 2000/60/EC and 2008/105/EC as regards priority substances in the field of water policy (31.01.2012), 2011, pp. 876.
[35] A.B. Boxall, C.J. Sinclair, K. Fenner, D. Kolpin, S.J. Maund, Environ. Sci. Technol. 38 (2004) 368A–375A.
[36] D. Fatta-Kassinos, M. Vasquez, K. Kümmerer, Chemosphere 85 (2011) 693–709.
[37] A. Achilleos, E. Hapeshi, N. Xekoukoulotakis, D. Mantzavinos, D. Fatta-Kassinos, Sep. Sci. Technol. 45 (2010) 1564–1570.
[38] A. Achilleos, E. Hapeshi, N.P. Xekoukoulotakis, D. Mantzavinos, D. Fatta-Kassinos, Chem. Eng. J. 161 (2010) 53–59.
[39] C. Fotiadis, N.P. Xekoukoulotakis, D. Mantzavinos, Catal. Today 124 (2007) 247–253.
[40] T. Kimura, T. Sakamoto, J. Leveque, H. Sohmiya, M. Fujita, S. Ikeda, T. Ando, Ultrason. Sonochem. 3 (1996) S157–S161.
[41] E. Hapeshi, A. Achilleos, A. Papaioannou, L. Valanidou, N.P. Xekoukoulotakis, D. Mantzavinos, D. Fatta-Kassinos, Sonochemical degradation of ofloxacin in aqueous solutions, Water Sci. Technol. 61 (2010) 3141–3146.
[42] ISO 6341:1996, Water Quality-Determination of the Inhibition of the Mobility of *Daphnia magna* Straus (Cladocera, Crustacea)-Acute Toxicity Test.
[43] I. Michael, E. Hapeshi, C. Michael, D. Fatta-Kassinos, Water Res. 44 (2010) 5450–5462.
[44] L.A. Pérez-Estrada, S. Malato, W. Gernjak, A. Agüera, E.M. Thurman, I. Ferrer, A.R. Fernández-Alba, Environ. Sci. Technol. 39 (2005) 8300–8306.
[45] M. Mrowetz, C. Pirola, E. Selli, Ultrason. Sonochem. 10 (2003) 247–254.
[46] C. Berberidou, I. Poulios, N. Xekoukoulotakis, D. Mantzavinos, Appl. Catal., B: Environ. 74 (2007) 63–72.
[47] D. Lambropoulou, I. Konstantinou, T. Albanis, A. Fernández-Alba, Chemosphere 83 (2011) 367–378.
[48] M. Stumpf, T.A. Ternes, K. Haberer, W. Baumann, Vom Wasser 91 (1998) 291–303.
[49] S. Weigel, U. Berger, E. Jensen, R. Kallenborn, H. Thoresen, H. Hühnerfuss, Chemosphere 56 (2004) 583–592.
[50] D. Bendz, N.A. Paxeus, T.R. Ginn, F.J. Loge, J. Hazard. Mater. 122 (2005) 195–204.
[51] J.B. Quintana, S. Weiss, T. Reemtsma, Water Res. 39 (2005) 2654–2664.
[52] C. Zwiener, S. Seeger, T. Glauner, F. Frimmel, Anal. Bioanal. Chem. 372 (2002) 569–575.
[53] L. Ferrando-Climent, N. Collado, G. Buttiglieri, M. Gros, I. Rodriguez-Roda, S. Rodriguez-Mozaz, D. Barceló, Sci. Total Environ. 438 (2012) 404–413.
[54] B. Zheng, Z. Zheng, J. Zhang, X. Luo, J. Wang, Q. Liu, L. Wang, Desalination 276 (2011) 379–385.
[55] G. Caviglioli, P. Valeria, P. Brunella, C. Sergio, A. Attilia, B. Gaetano, J. Pharm. Biomed. Anal. 30 (2002) 499–509.
[56] M. Skoumal, R.M. Rodríguez, P.L. Cabot, F. Centellas, J.A. Garrido, C. Arias, E. Brillas, Electrochim. Acta 54 (2009) 2077–2085.
[57] M. Schmitt-Jansen, P. Bartels, N. Adler, R. Altenburger, Anal. Bioanal. Chem. 387 (2007) 1389–1396.
[58] T. Schulze, S. Weiss, E. Schymanski, P.C. von der Ohe, M. Schmitt-Jansen, R. Altenburger, G. Streck, W. Brack, Environ. Pollut. 158 (2010) 1461–1466.
[59] X. Zhao, Y. Hou, H. Liu, Z. Qiang, J. Qu, Electrochim. Acta 54 (2009) 4172–4179.
[60] J. Hofmann, U. Freier, M. Wecks, S. Hohmann, Appl. Catal., B: Environ. 70 (2007) 447–451.
[61] T. Leemann, C. Transon, P. Dayer, Life Sci. 52 (1993) 29–34.
[62] S. Shen, M.R. Marchick, M.R. Davis, G.A. Doss, L.R. Pohl, Chem. Res. Toxicol. 12 (1999) 214–222.
[63] H. Yu, E. Nie, J. Xu, S. Yan, W.J. Cooper, W. Song, Water Res. 47 (2013) 1909–1918.
[64] H. Lee, E. Lee, S. Yoon, H. Chang, K. Kim, J. Kwon, Chemosphere 87 (2012) 969–974.
[65] M. Soufan, M. Deborde, B. Legube, Water Res. 46 (2012) 3377–3386.
[66] C. Wang, G. Lu, Y. Li, Bull. Environ. Contam. Toxicol. 75 (2005) 102–108.
[67] E. Illes, E. Takacs, A. Dombi, K. Gajda-Schrantz, G. Racz, K. Gonter, L. Wojnárovits, Sci. Total Environ. 447 (2013) 286–292.
[68] J. Castell, M. Miranda, I. Morera, Photochem. Photobiol. 46 (1987) 991–996.
[69] M. Miranda, I. Morera, F. Vargas, M. Gómez-Lechón, J. Castell, Toxicol. in Vitro 5 (1991) 451–455.
[70] G. Rácz, Z. Csenki, R. Kovács, Á. Hegyi, F. Baska, L. Sujbert, I. Zsákovics, R. Kis, R. Gustafson, B. Urbányi, Pathol. Oncol. Res. 18 (2012) 579–584.
[71] L. Rizzo, S. Meric, D. Kassinos, M. Guida, F. Russo, V. Belgiorn, Water Res. 43 (2009) 979–988.